Ocean Dynamics (2020) 70:991–1003
https://doi.org/10.1007/s10236-020-01379-z

Modeling the ice-attenuated waves in the Great Lakes

Peng Bai[1,2] · Jia Wang[2] · Philip Chu[2] · Nathan Hawley[2] · Ayumi Fujisaki-Manome[3,4] · James Kessler[2] · Brent M. Lofgren[2] · Dmitry Beletsky[3] · Eric J. Anderson[2] · Yaru Li[3]

Received: 12 January 2020 / Accepted: 23 April 2020 / Published online: 29 May 2020

Abstract

A partly coupled wave-ice model with the ability to resolve ice-induced attenuation on waves was developed using the Finite-Volume Community Ocean Model (FVCOM) framework and applied to the Great Lakes. Seven simple, flexible, and efficient parameterization schemes originating from the WAVEWATCH III® IC4 were used to quantify the wave energy loss during wave propagation under ice. The reductions of wind energy input and wave energy dissipation via whitecapping and breaking due to presence of ice were also implemented (i.e., blocking effect). The model showed satisfactory performance when validated by buoy-observed significant wave height in ice-free season at eight stations and satellite-retrieved ice concentration. The simulation ran over the basin-scale, five-lake computational grid provided a whole map of ice-induced wave attenuation in the heavy-ice year 2014, suggesting that except Lake Ontario and central Lake Michigan, lake ice almost completely inhibited waves in the Great Lakes under heavy-ice condition. A practical application of the model in February 2011 revealed that the model could accurately reproduce the ice-attenuated waves when validated by wave observations from bottom-moored acoustic wave and current profiler (AWAC); moreover, the AWAC wave data showed quick responses between waves and ice, suggesting a sensitive relationship between waves and ice and arguing that accurate ice modeling was necessary for quantifying wave-ice interaction.

Keywords Great Lakes · Wave dynamics · Ice-induced wave attenuation · FVCOM–SWAVE–UG-CICE

1 Introduction

Extending approximately from 76.0 ° W to 92.1 ° W in longitude and 41.4 ° N to 49.0 ° N in latitude, the Laurentian Great Lakes (Great Lakes) are the largest group of fresh water lakes on the Earth (Fig. 1a). The Great Lakes comprise about 1/5 of the world's surface freshwater, and nearly 1/8 of the American population and 1/3 of the Canadian population live within their watershed. With large dimensions in addition to complex geometry and topography, the Great Lakes present sea-like hydrodynamics under sustained atmospheric forcing (Beletsky et al. 1999; Schwab and Beletsky 2003; Wang et al. 2012; Bai et al. 2013).

Genesis and melting of ice on the Great Lakes directly modify the hydrodynamic processes, the thermal structure, and the adjacent atmospheric boundary layer, mainly through three physical mechanisms: weakening surface wind stress; generating higher albedo than over open waters; and modifying heat and moisture exchange processes between lake and atmosphere (Xue et al. 2017), which, in turn, affects the lake ecosystem (Vanderploeg et al. 1992; Brown et al. 1993), economy (Niimi 1982), and water level variability (Sellinger et al. 2007). Lake ice coverage is characterized by large interannual variability (Fig. 1b) and is sensitive to the modulation of teleconnection patterns such as the Arctic Oscillation and the El Niño-Southern Oscillation (Wang et al. 2012; Bai et al. 2012, 2015). Lake ice also plays a vital role in regional climate, for example, modulating the lake-effect snowfall (Wright et al. 2013; Vavrus et al. 2013).

Forced by winds, surface gravity waves generated on the Great Lakes become one of the dominant driving forces for lake hydrodynamics (Hubertz et al. 1991; Niu and Xia 2016;

This article is part of the Topical Collection on the *11th International Workshop on Modeling the Ocean (IWMO), Wuxi, China, 17-20 June 2019*

Responsible Editor: Tal Ezer

✉ Peng Bai
peng.bai@noaa.gov; baip@gdou.edu.cn

[1] College of Ocean and Meteorology, Guangdong Ocean University, Zhanjiang 524088, Guangdong, China

[2] Great Lakes Environmental Research Laboratory, NOAA, Ann Arbor, MI 48108, USA

[3] Cooperative Institute for Great Lakes Research, University of Michigan, Ann Arbor, MI 48108, USA

[4] Department of Climate and Space Sciences and Engineering, University of Michigan, Ann Arbor, MI 48104, USA

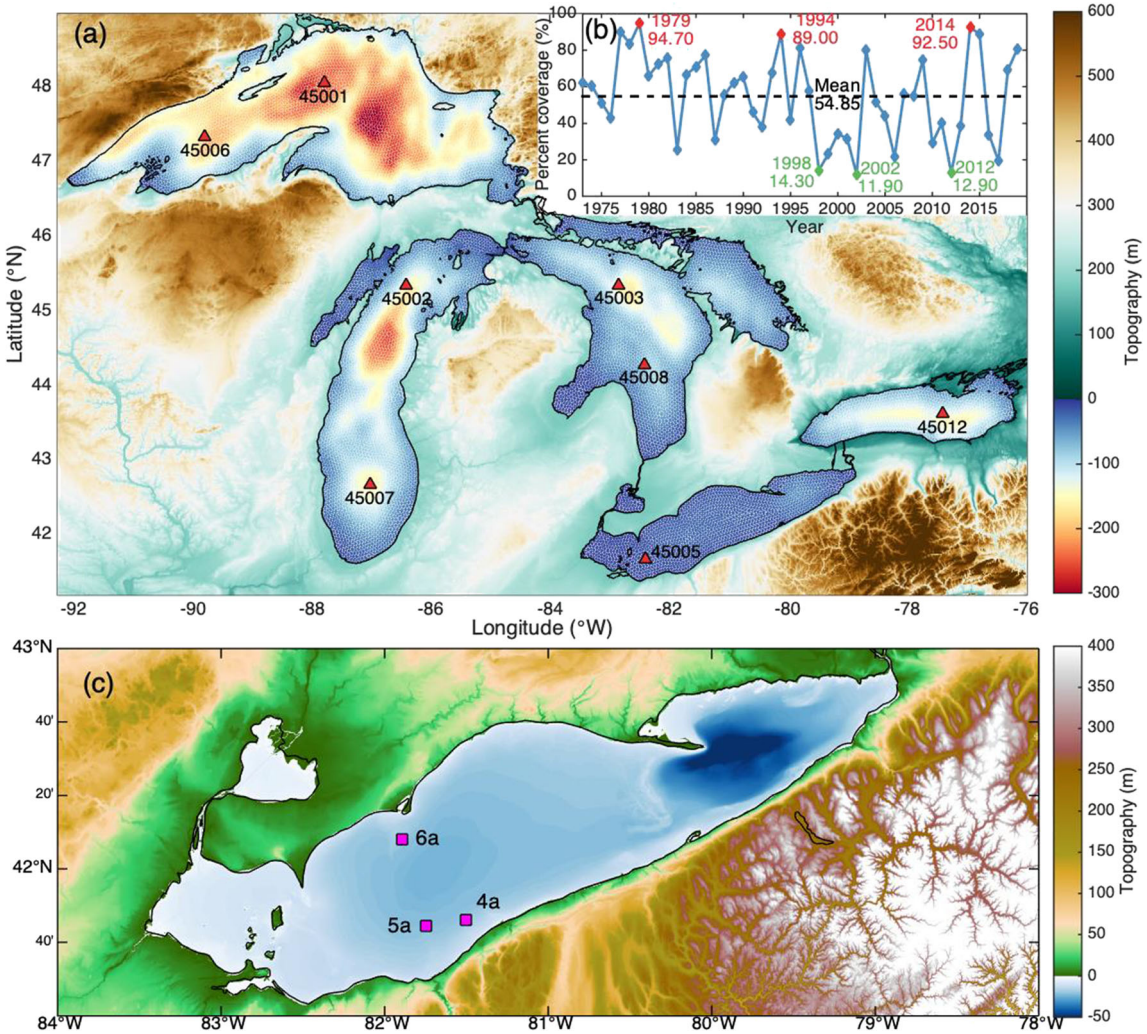

Fig. 1 Topography and FVCOM computational meshes for the Great Lakes (**a**), red triangles show locations of the NDBC buoys. Great Lakes annual maximum ice coverage from 1973 to 2019 (**b**). AWAC mooring locations (purple squares) in Lake Erie (**c**)

Mao and Xia 2017). Waves can interact with currents, leading to stronger bottom shear stress, enhancing the vertical mixing and supplying additional momentum flux to the mean circulation. Conversely, in addition to exerting refraction, modification of bottom stress, and blocking effects on the waves (Vincent 1979; Ris et al. 1999; Ardhuin et al. 2012), currents could also change the wave frequency through Doppler shift; meanwhile, variations in the water level could change the water depth felt by the waves (Pleskachevsky et al. 2009). Lake waves and lake circulation form a complicated feedback system. For example, Brissette et al. (1993) revealed that current-induced refraction can lead to significant difference between the wind and wave directions in Lake St. Clair. Wave-current interaction is found to play a critical role in sediment resuspension and transport processes in Lake Michigan by modifying the bottom shear stress (Lou et al. 2000). Bai et al. (2013) suggested that wave mixing is a key dynamical driver for lake thermal structure. Numerical investigation by Niu and Xia (2017) indicated that, in Lake Erie, wave-enhanced surface stress can significantly modulate the surges, offshore currents, and thermal structures.

During the ice season, lake waves generated in the open waters can penetrate into the ice-covered region, causing interaction between waves and ice. Part of the wave energy is reflected at the waterward periphery of the ice, and the remaining energy, together with the winds and currents, would act on the ice mechanically, modifying the growth process and hence the morphology and structure of the ice cover, weakening and rupturing the ice (Squire 2007; Barber et al. 2009; Vaughan and Squire 2011; Dumont et al. 2011; Williams et al. 2013; Kohout et al. 2016). On the other hand, ice modulates the waves mainly through three physical mechanisms: (1) attenuation owing to the energy transfer and dissipation during wave-ice interaction; (2) scattering caused by energy reflection at the ice edge; and (3) refraction due to different dispersion relations in the open seas and the ice-covered waters. Observations show that ice is often heterogeneous in nature and varied in form, which strongly impacts wave-ice

interaction (e.g., Campbell et al. 2014). Wave propagation in ice is extensively investigated by employing various scattering or viscous models. In scattering models, wave energy is reduced by accumulations of the partial energy reflections occurring when waves encounter a floe edge, and therefore, scattering models depend strongly on the distance waves traveling into the ice-covered waters and the distribution of ice floe size (Kohout and Meylan 2008; Bennetts and Squire 2009; Bennetts and Squire 2011; Williams et al. 2013). In viscous models, wave energy is decreased by viscous dissipation, and hence, these models are independent of the floe size (Wang and Shen 2011; De Santi et al. 2018).

Understanding the wave-ice-lake interrelations is necessary for guiding proper navigation, engineering, hazard warning, and regulatory actions in the Great Lakes. Previous investigations have explored and emphasized the vital roles of wave-lake interactions in the Great Lakes (e.g., Niu and Xia 2017; Mao and Xia 2017). However, we still have poor knowledge about how waves and ice interact with each other in the Great Lakes. In this paper, we developed a partly coupled wave-ice interaction model that able to describe the ice-induced wave attenuation within the Finite Volume Community Ocean Model (FVCOM) framework, and then we applied the model to the Great Lakes.

The outline of the paper is as follows. Section 2 describes the model, parameterization schemes quantifying ice-induced wave attenuation, model configuration, numerical experiments, and observational data; in Sect. 3, a modeling estimation of ice-induced wave attenuation in the Great Lakes during heavy-ice year 2014 is presented; in Sect. 4, a practical application of the coupled wave-ice-lake model in February 2011 is demonstrated; and in Sect. 5, the major conclusions are summarized.

2 Data and methodology

2.1 FVCOM–SWAVE–UG-CICE

We used FVCOM (Chen et al. 2003), which is capable of resolving the complex topography in the Great Lakes, to model the lake waves (FVCOM-SWAVE, Qi et al. 2009) and ice (UG-CICE, Gao et al. 2011). FVCOM-SWAVE is a finite-volume unstructured-grid third-generation wave model evolved from the Simulating WAves Nearshore (SWAN, Booij et al. 1999), which models the wave generation, propagation, dissipation, refraction, and nonlinear wave-wave interactions by solving the wave action balance equation expressed as:

$$\frac{\partial N}{\partial t}+\nabla\cdot\left[\left(\vec{\mathbf{c}_g}+\vec{\mathbf{U}}\right)N\right]+\frac{\partial C_\sigma N}{\partial\sigma}+\frac{\partial C_\theta N}{\partial\theta}=\frac{S_{\text{in}}+S_{\text{nl}}+S_{\text{ds}}}{\sigma},\quad(1)$$

where N stands for the wave action density spectrum, t represents the time, $\vec{\mathbf{c}_g}$ is the wave group velocity, $\vec{\mathbf{U}}$ is the ambient flow velocity vector, σ and θ are the intrinsic frequency and wave direction, C_σ and C_θ are the wave propagation velocities in spectral space (σ, θ), S_{in} is the wind energy input, S_{nl} is the energy transfer due to nonlinear wave-wave interactions among spectral components, and S_{ds} is the wave decay through wave breaking ($S_{\text{ds, br}}$), whitecapping ($S_{\text{ds, w}}$), and bottom friction ($S_{\text{ds, b}}$).

Presence of ice would inhibit the energy input by winds and restrain the wave energy decay via whitecapping and breaking; therefore, these three source-sink terms are scaled by the open water fraction (hereinafter, the blocking effect). Meanwhile, the terms associated with the nonlinear wave-wave interactions and bottom friction remain the same as that in open waters. Hence, wave propagation through ice-covered waters is governed by:

$$\frac{\partial N}{\partial t}+\nabla\cdot\left[\left(\vec{\mathbf{c}_g}+\vec{\mathbf{U}}\right)N\right]+\frac{\partial C_\sigma N}{\partial\sigma}+\frac{\partial C_\theta N}{\partial\theta}=\frac{(1-C_{\text{ice}})\left(S_{\text{in}}+S_{\text{ds,w}}+S_{\text{ds,br}}\right)+S_{\text{nl}}+S_{\text{ds,b}}+S_{\text{ice}}}{\sigma},\quad(2)$$

where C_{ice} is the ice concentration, $S_{\text{ice}}=-\alpha EC_g$ is a new wave energy sink term due to the damping of ice cover, in which α is attenuation coefficient, E is wave spectral density, and C_g is wave group velocity.

The FVCOM includes an internally coupled ice model, the UG-CICE, which was employed in this study to simulate the lake ice dynamics. UG-CICE is an unstructured-grid, finite-volume version of the Los Alamos Community Ice Code (CICE, Hunke et al. 2010) implemented into the FVCOM framework by Gao et al. (2011); it employs the same governing equations as the CICE, has been widely applied to many cold regions including the Great Lakes, and showed satisfactory performance (e.g., Gao et al. 2011; Fujisaki-Manome and Wang 2016; Zhang et al. 2016; Anderson et al. 2018).

2.2 Parameterizing schemes for estimating attenuation coefficient α

Many efforts have been dedicated to quantifying ice-induced attenuation coefficient, i.e., α (e.g., Wadhams et al. 1988; Kohout et al. 2007, 2014; Kohout and Meylan 2008; Meylan et al. 2014; Doble et al. 2015; Rogers et al. 2016). However, some of the proposed theories are based on a fluid-solid interactive frame, and the solving processes are complicated and inefficient and therefore are difficult to implement in a wave-ice interaction model. In IC4 of WAVEWATCH III, seven simple, flexible, and efficient empirical schemes (IC4M1–M7) are given for evaluating α, which had been referred and transplanted to the FVCOM-SWAVE in this study.

The origins and formulas of IC4M1–M7 are summarized as Table 1. The IC4M1 is exponential as a function of wave period, and the coefficients were obtained via an exponential fit to the observations from Wadhams et al. (1988). The IC4M2 is a 4th degree polynomial fit between α and wave period based on the measured wave attenuation in the Antarctic by Meylan et al. (2014). Kohout and Meylan (2008) developed a scattering model to calculate wave attenuation, and based on their results, Horvat and Tziperman (2015) utilized a quadratic equation to fit α, wave period, and ice thickness, i.e., the IC4M3. Kohout et al. (2014) analyzed the same measurements by Meylan et al. (2014) and found that α is a piecewise function of significant wave height and is independent of wave frequency, i.e., IC4M4. The IC4M5 is a step function in frequency space with four steps (Doble et al. 2015), and the IC4M6 is identical to IC4M5 but with several differences (Rogers et al. 2016), for example, IC4M6 allows up to 10 steps. For the IC4M7, it is a formula that depends on wave frequency and ice thickness developed by Doble et al. (2015) using the data collected in the Weddell Sea. Further details are found in Collins and Rogers (2017) and the WAVEWATCH III® Development Group (2016).

Figure 2 shows the relationships between attenuation coefficient α and wave periods produced by IC4M1–M7. The higher frequency the waves, the stronger damping by the ice, which suggests that ice generally acts as a low-pass filter for wave energy (e.g., Squire 2007; Collins and Rogers 2017). The IC4M3 and IC4M7 consider ice thickness as a vital factor impacting the α, demonstrating that thicker ice has stronger damping ability on waves (Fig. 2b), while IC4M4 reveals stronger waves lose less energy when they pass through ice covered region (Fig. 2c). As Fig. 2 reveals, magnitudes of α estimated by different parameterization schemes could differ by several orders, mainly due to the different ice and wave conditions based on which IC4M1–M7 were obtained.

2.3 Model configuration and numerical experiments

Simulations of lake circulation, waves, and ice were carried out over the same model domain with the Great Lakes-FVCOM (Great Lakes Finite Volume Coastal Ocean Model, developed by Bai et al. 2013), and as Fig. 1a shows, the computational mesh covered the entire Great Lakes. Only water exchange between Lakes Michigan and Huron was allowed, while other lakes were kept separated due to narrow passages between them. The averaged horizontal resolution of this unstructured triangular grid was ~3.5 km, and in the vertical direction, a 21-layer terrain-following coordinate with higher

Table 1 Summary of the origins and formulas in IC4, where α is attenuation coefficient, T denotes wave period, H_i is ice thickness, SWH is significant wave height, and f is wave frequency

Method	Reference	Formula
IC4M1	Wadhams et al. (1988)	$\alpha = e^{(-0.18 * T - 0.73)}$
IC4M2	Meylan et al. (2014)	$\alpha = \frac{2.12*10^{-3}}{T^2} + \frac{4.59*10^{-2}}{T^4}$
IC4M3	Kohout and Meylan (2008) Horvat and Tziperman (2015)	$\alpha = e^{\left(-0.3203+2.058H_i-0.9375T-0.4269{H_i}^2+0.1566H_iT+0.0006T^2\right)}$
IC4M4	Kohout et al. (2014)	$\alpha = \begin{cases} 2*5.35*10^{-6}\ (\mathrm{SWH}\le 3) \\ \frac{2*16.05*10^{-6}}{\mathrm{SWH}}\ (\mathrm{SWH} > 3) \end{cases}$
IC4M5	Doble et al. (2015)	$\alpha = \begin{cases} 2*5.0*10^{-6}\ (f < 0.1) \\ 2*7.0*10^{-6}\ (0.1 \le f < 0.12) \\ 2*1.5*10^{-5}\ (0.12 \le f < 0.16) \\ 2*1.0*10^{-4}\ (f \ge 0.16) \end{cases}$
IC4M6 (IC4M6H)	Rogers et al. (2016)	$\alpha = \begin{cases} 2*2.94*10^{-6}\ (f < 0.1) \\ 2*4.27*10^{-6}\ (0.1 \le f < 0.15) \\ 2*7.95*10^{-6}\ (0.15 \le f < 0.20) \\ 2*2.95*10^{-5}\ (0.20 \le f < 0.25) \\ 2*1.12*10^{-4}\ (0.25 \le f < 0.30) \\ 2*2.74*10^{-4}\ (0.30 \le f < 0.35) \\ 2*4.95*10^{-4}\ (0.35 \le f < 0.40) \\ 2*8.94*10^{-4}\ (f \ge 0.40) \end{cases}$
IC4M7	Doble et al. (2015)	$\alpha = 0.2 * T^{-2.13} * H_i$

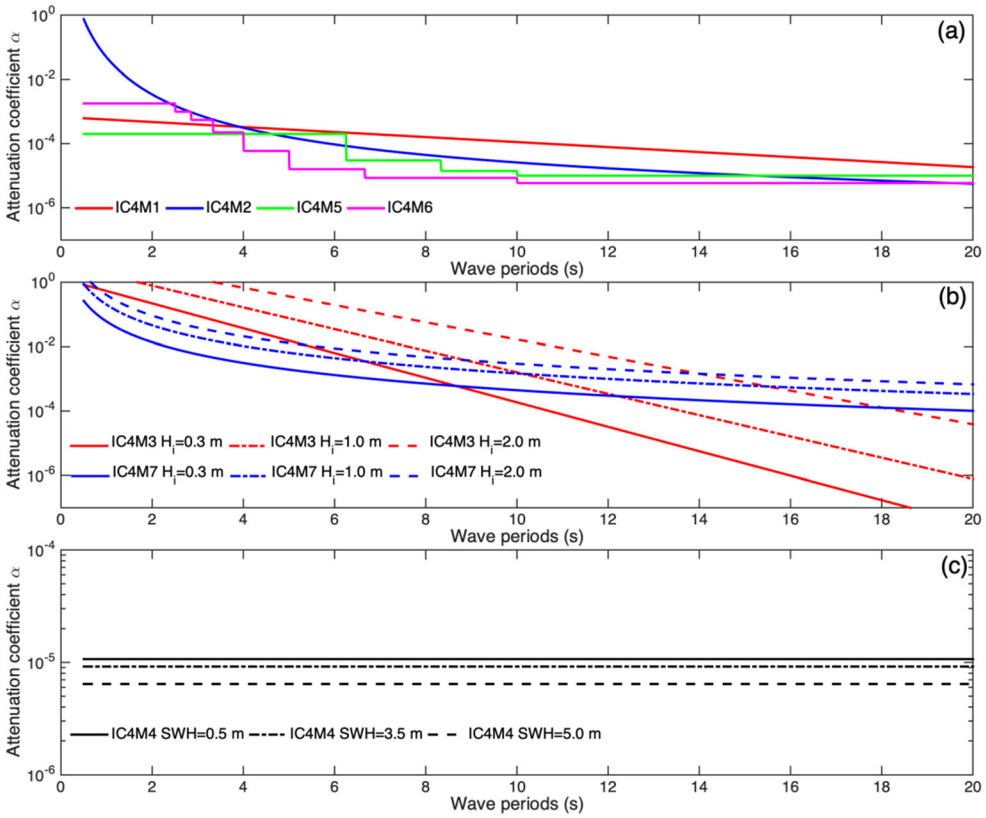

Fig. 2 Attenuation coefficient α against the wave periods T ($\alpha = f(T)$) based on IC4M1, IC4M2, IC4M5, and IC4M6 (**a**). Attenuation coefficient α against the wave periods and ice thickness H_i ($\alpha = f(T, H_i)$) given by IC4M3 and IC4M7 (**b**). Attenuation coefficient α against the wave periods and significant wave height SWH ($\alpha = f(T, \mathrm{SWH})$) following IC4M4 (**c**)

resolution placed near the surface and bottom was adopted. The minimum depth was set to 10 m to ensure global stability, i.e., $h + \zeta > 0$ (h is the undisturbed water depth and ζ is the free surface elevation, Wang 1996). In this study, the leapfrog (centered differencing) scheme for time discretization was used to replace the Euler forward scheme in the internal mode and the Euler forward Runge-Kutta scheme in the external mode in the integral equations. The reason is that the two-time-step Euler forward scheme has been proven inertially unstable, while the leapfrog scheme is inertially neutral stable (Wang and Ikeda 1997a, 1997b; Wang et al. 2020, this issue). Lake circulation, waves, and the ice were driven by the 3-hourly North American Regional Reanalysis (NARR) product, a long-term set of consistent climate data covering all of North and Central America with a 32-km horizontal resolution (Mesinger et al. 2006). The wave module resolved wave spectral frequency with 40 frequency bins ranging from 0.04 to 1 Hz (1 Hz = 1/s) and applied a full cycle direction spectrum with 36 directional bands. Exponential wave growth and whitecapping functions based on Komen et al. (1984), bottom friction parameterization scheme from Madsen et al. (1989), and quadruplet wave-wave interactions following Hasselmann et al. (1973) were utilized. In the circulation module, time step for the internal mode was 60 s and a splitting ratio of 20 was used; meanwhile, a 60-s time step was adopted for the ice and wave modules.

A set of numerical experiments designed as Table 2 were conducted to explore the ice-induced wave attenuation in the Great Lakes. In Table 2, EXP0 was a wave-only modeling case, it was used to examine the performance of the wave module during ice-free season, and it also provided a reference for those experiments with ice-induced wave attenuation during the ice season. EXP1–EXP7 were coupled wave-ice modeling cases with both blocking effect and ice-induced wave attenuation, and they used IC4M1–IC4M7 to quantify wave attenuation by ice, respectively. The modeling period of EXP0–EXP7 were in 2014 because 2014 is a "big chill" year (Fig. 1b) and better understanding of the wave-ice interaction under extreme climate conditions is important. EXP8 was identical to EXP0, which was a wave-only modeling case. For the EXP9, it was a coupled wave-ice modeling experiment using IC4M6 to calculate ice-induced wave attenuation; meanwhile, blocking effect was also considered. However, the modeling periods of EXP8 and EXP9 were in 2011, when there were available wave data observed during the ice season, which therefore could evaluate the performance of the partly coupled wave-ice model. All numerical runs were initialized from a motionless state. To focus on the ice-induced wave

Table 2 Numerical experiments design of this study

Case	Method quantifying α	Modeling period	Note
EXP0	N/A	2014.01.01–2014.12.31	Wave-only modeling
EXP1	IC4M1	2014.01.01–2014.06.30	Coupled wave-ice modeling with both blocking effect and ice-induced wave attenuation
EXP2	IC4M2		
EXP3	IC4M3		
EXP4	IC4M4		
EXP5	IC4M5		
EXP6	IC4M6		
EXP7	IC4M7		
EXP8	N/A	2011.01.01–2011.03.03	Wave-only modeling
EXP9	IC4M6	2011.01.01–2011.03.03	Coupled wave-ice modeling with both blocking effect and ice-induced wave attenuation

attenuation, the feedback from waves to ice, and the dynamics related with wave-current interaction were not considered during current stage.

2.4 Observational data

To assess the model's performance in simulating wave dynamics in Great Lakes, the significant wave height (SWH) in 2014 observed by eight buoys 45001–45003, 45005–45008, and 45012 (https://www.ndbc.noaa.gov/) were utilized to validate the modeled SWH, and the buoy locations are illustrated in Fig. 1a. Meanwhile, the buoy-observed lake surface winds were used to evaluate the quality of the NARR 3-hourly winds over the Great Lakes.

We used the satellite-retrieved ice concentration data, a product based on multi-satellite observations (e.g., Radarsat-2, Envisat, AVHRR, GOES, and MODIS) derived from the National Ice Center (NIC) Great Lakes Ice Analysis Charts managed and provided by the NOAA Great Lakes Environmental Research Laboratory (https://www.glerl.noaa.gov/), to appraise the model's ability in the Great Lakes ice dynamics.

Wave data measured using the Nortek AWAC (acoustic wave and current profiler) at three stations 4a, 5a, and 6a in Lake Erie (locations in Fig. 1c) during February 2011 were employed to evaluate the performance of the coupled ice-wave modeling, further details of these wave data are available in Hawley et al. (2018).

3 Modeling the ice-attenuated waves in 2014

3.1 Model performance in wave simulation

In the form of scatter diagrams, comparisons between the simulated SWH and the ones observed by NDBC buoys at eight stations are shown in Fig. 3. Valid wave observations from the NDBC buoys were only available during ice-free time, generally from the mid May to late November, 2014. Figure 3 reveals that the modeled SWH were reasonably consistent with the observed ones. To further evaluate the model's performance in simulating lake waves, correlation coefficients (CC), root mean square error (RMSE), and mean absolute error (MAE) were applied, and the definitions are given below:

$$\mathrm{CC} = \frac{\sum_{i=1}^{N}(x_i - x)(y_i - y)}{\sqrt{\frac{1}{N}\sum_{i=1}^{N}(x_i - x)^2}\sqrt{\frac{1}{N}\sum_{i=1}^{N}(y_i - y)^2}}, \tag{3}$$

$$\mathrm{RMSE} = \sqrt{\frac{1}{N}\sum_{i=1}^{N}(x_i - y_i)^2}, \tag{4}$$

$$\mathrm{MAE} = \frac{1}{N}\sum_{i=1}^{N}|x_i - y_i|, \tag{5}$$

where N is the total sampling number, x_i and y_i ($i = 1, 2, 3, \ldots, N\text{-}1, N$) are the observed and simulated time series of SWH, and over bars donate average of the time series. CC, RMSE, and MAE correspond to the comparisons at different buoy stations are shown in the subfigures of Fig. 3, respectively, and overall, CC, RMSE, and MAE for all eight comparisons were respectively 0.77, 0.38, and 0.26 m, and were comparable with former wave simulations for the Great Lakes using third-generation wave models (e.g., Moeini and Etemad-Shahidi 2007; Mao et al. 2016; Niu and Xia 2016). Without any calibration, such performance of the wave module was generally satisfactory and was eligible if for use as the basis of coupled wave-ice modeling.

Comparisons[1] between the NARR winds and the NDBC buoy-observed winds revealed that the averaged differences in wind speed (WSPD) between the NARR winds and winds observed by NDBC buoys 45001–45003, 45005–45008, and 45012 ($\mathrm{WSPD_{Buoy}}$–$\mathrm{WSPD_{NARR}}$) in 2014 were − 0.43, 0.53, 0.47, 0.87, 0.68, 0.28, 0.84, and 0.85 m/s, respectively,

[1] Anemometer heights above the ground of NDBC buoys 45001–45003, 45005–45008, and 45012 are 5 m, the NARR winds at 10 m were used to force the model, thus the buoy-observed winds were converted to winds at 10 m following a logarithmic relationship for wind speed profile (Allen et al. 1998).

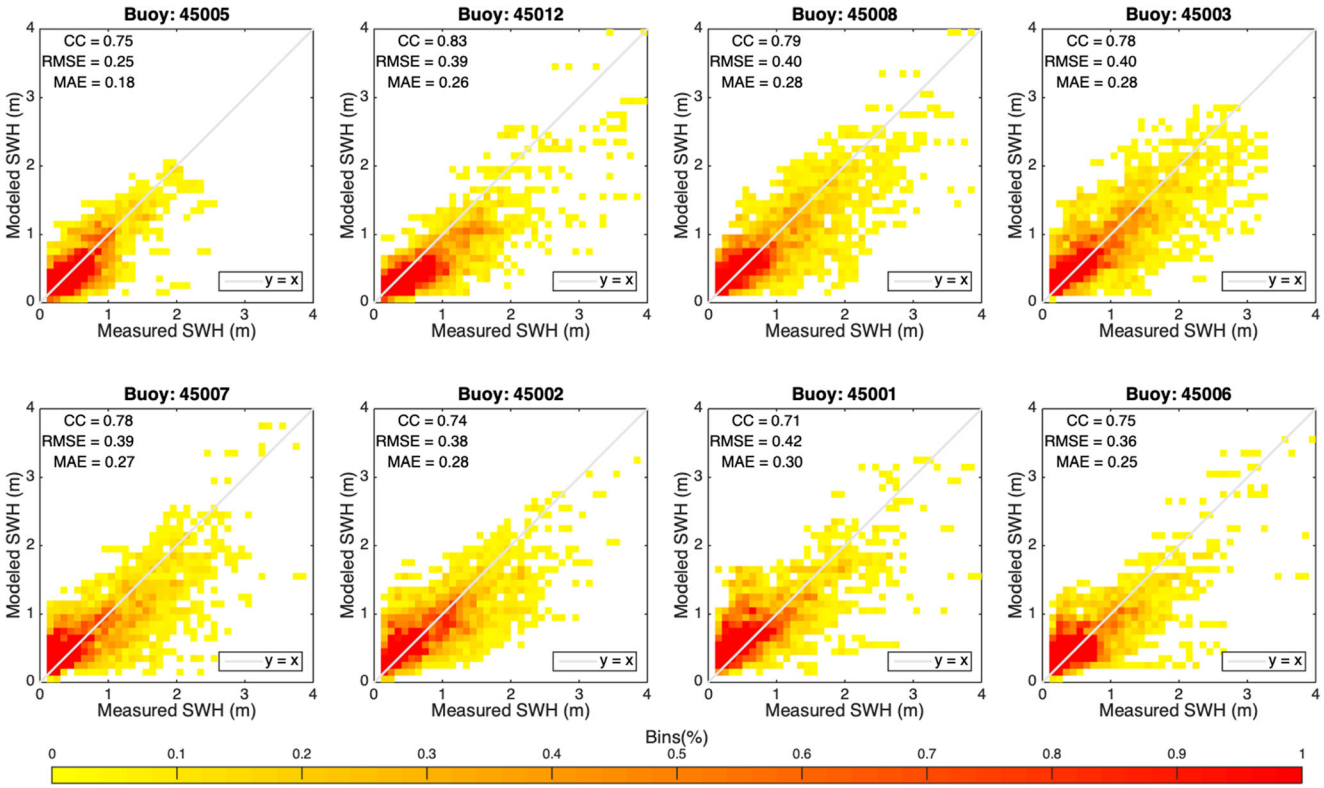

Fig. 3 Scatter diagrams of significant wave height: modeled results against the NDBC buoy observations. Scatter diagrams are created by binning the data into 0.1-m bins, and the gray line indicates function $y = x$. Model results are from numerical experiment EXP0 (a wave-only case)

suggesting that the model wind forcing (NARR product) generally underestimated the intensity of lake surface winds (Fig. 4). Mao et al. (2016) examined the impacts of three different wind field sources on wave dynamics in Lake Michigan; their results demonstrated that accuracy of wind forcing is the key factor determining model's performance for waves. Therefore, the relatively weak NARR winds with low spatiotemporal resolution misjudged the real wind field by a certain extent, which was one of the reasons for the errors displayed in Fig. 3. In addition to the wind forcing, as many previous studies revealed, accuracy of the model bathymetry, resolution and design of the computational grid, choice of formulations describing the wind input, whitecapping, and depth-induced wave breaking, as well as consideration of wave-current interaction, all could affect the wave model's performance in the Great Lakes (e.g., Mao et al. 2016; Niu and Xia 2016; Mao and Xia 2017).

3.2 Model performance in ice modeling

As illustrated in Sect. 2.2, ice characteristics, including ice concentration and ice thickness, are the vital parameters determining ice ability to attenuate waves, and therefore, it is necessary to evaluate model's performance in simulating lake ice. Using the satellite-measured ice concentration from the NIC, the modeled spatial distribution of ice concentration over the Great Lakes in February and March 2014 were examined.

Observations showed that Lakes Superior, Huron, and Erie were almost fully covered by ice (Fig. 5 a and b), while there was less ice in Lake Michigan (particularly in the central lake) with ice concentration ranging from 20 to 50% in most parts. In Lake Ontario, the whole lake was nearly ice free, which was just as indicated by previous studies (Wang et al. 2018). The various ice dynamics in different lakes are mainly caused by the spatially different climate forcing over each lake; meanwhile, lake ice will respond differently even to the same climate forcing depending on each lake's orientation, topography, and turbidity as revealed by Wang et al. (2018). As demonstrated by Fig. 5, the modeled ice concentration was reasonably consistent with the satellite observations in the form of intensity as well as the spatial distribution; furthermore, observations revealed increased ice concentration from February to March, 2014 (Fig. 5 a and b), and this tendency was well reproduced by the model (Fig. 5 c and d), suggesting reliable model performance in simulating lake ice dynamics.

3.3 Ice-induced attenuation on lake waves

Based on EXP0–EXP7, ice-induced attenuation on lake waves in February 2014 was evaluated. Figure 6 a shows the

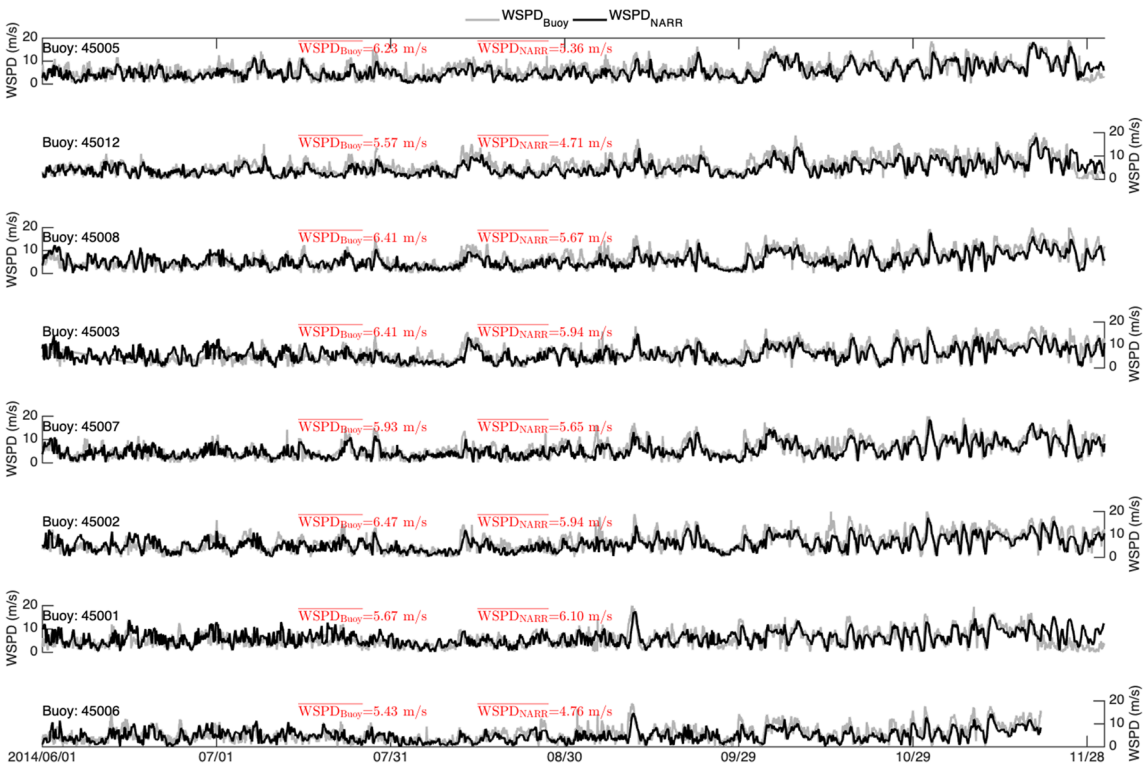

Fig. 4 Comparisons of the time series of wind speed between the NDBC buoy observations (gray lines) and the NARR product (black lines) during June 1 to December 1, 2014. The mean value of each wind speed time series is marked with red

monthly mean SWH in the Great Lakes based on EXP0, and the monthly averaged differences in SWH between EXP0 and EXP1–EXP7 are displayed in Fig. 6b–h, respectively. As suggested by Table 1 and Fig. 2, the ice-induced wave attenuations quantified by different methods in IC4 were different; meanwhile, the blocking effect of ice on waves remained the

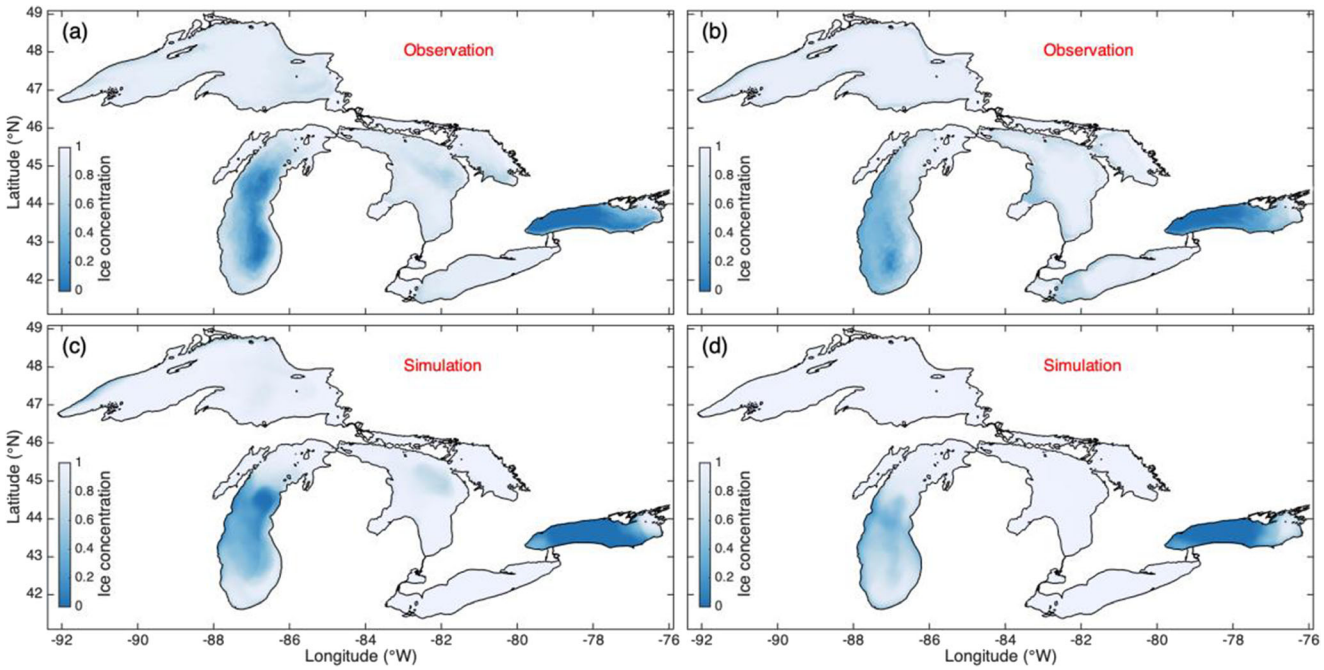

Fig. 5 The monthly mean NIC satellite-measured ice concentration over the Great Lakes in February (**a**) and March (**b**), 2014, respectively. The simulated spatial distribution of monthly averaged ice concentration over the Great Lakes in February (**c**) and March (**d**), 2014, successively

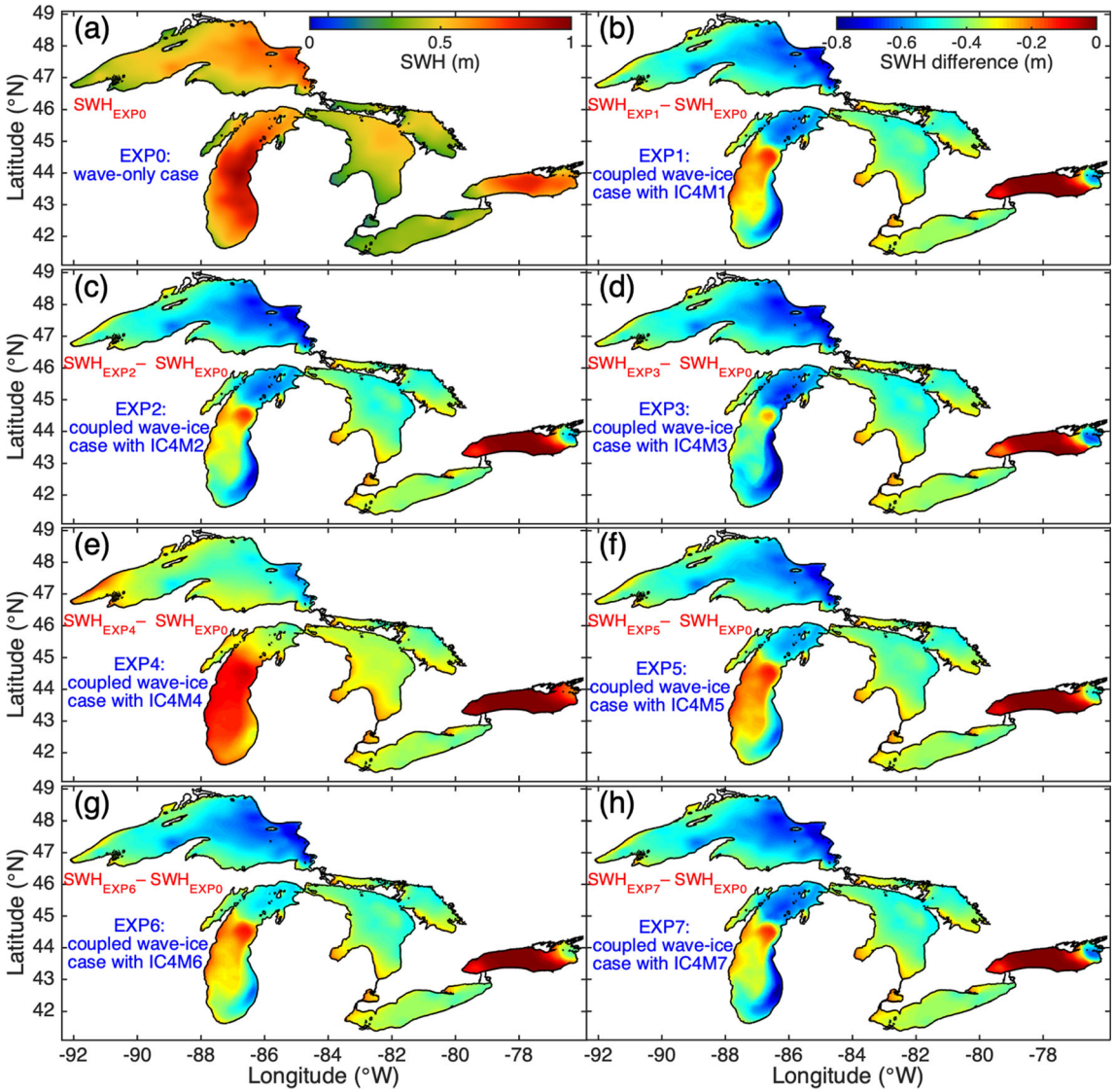

Fig. 6 Monthly mean SWH in the Great Lakes based on EXP0 for February 2014 (**a**). Monthly averaged differences in SWH between EXP0 and EXP1 (**b**), EXP2 (**c**), EXP3 (**d**), EXP4 (**e**), EXP5 (**f**), EXP6 (**g**), and EXP7 (**h**) in February 2014

same among different numerical runs; therefore, as revealed by Fig. 6b–h, the attenuation of waves by ice simulated by EXP1–EXP7 differed from each other.

Although EXP1–EXP7 simulated different values of wave attenuation, their spatial patterns were quite similar to each other. All reasonably revealed that wave attenuation by ice was positively correlated with ice concentration. Spatially averaged SWH decreased by 0.435, 0.446, 0.467, 0.324, 0.418, 0.424, and 0.450 m over the entire Great Lakes (except Lake Ontario) based on EXP1–EXP7, respectively. In most areas of Lakes Superior, Huron, and Erie, the reduction of SWH by heavy ice (Fig. 6b–h) and the SWH modeled by EXP0 (Fig. 6a) nearly canceled each other out, suggesting no wave would develop in these large lakes under heavy-ice condition. In the central basin of Lake Michigan, there was much less ice (Fig. 5), and the wave attenuation was estimated at approximately 0.2 m (Fig. 6b–h), which only counteracted minor parts of the SWH modeled by EXP0; therefore, significant wave motions still existed. The weakest wave attenuation was found in Lake Ontario, not surprisingly due to the mild lake ice there (Fig. 5).

Note that EXP3 (with IC4M3) and EXP7 (with IC4M7) produced the strongest attenuation (0.467 and 0.450 m); the modeled monthly mean ice thickness for February 2014 suggested approximately a 0.3-m thick ice over the Great Lakes; meanwhile, the typical wave period in winter was shorter than 4 s; thus, under such ice and wave conditions, the attenuation coefficients α given by IC4M3 and IC4M7 were generally larger than other schemes (Fig. 2), which well explains the stronger wave attenuation estimated by these two methods.

4 Practical application in 2011

The preceding results strongly indicated that wave-ice interaction over the Great Lakes plays a vital role in modifying the local hydrodynamic environment, particularly in the wave dynamics. However, lack of in situ data in 2014 makes it unable to evaluate the performance of the partly coupled wave-ice model developed in this study. To examine the reliability of this model, a practical application in the Great Lakes for February 2011 was conducted, during which period wave data observed by bottom-moored AWAC at three stations (Fig. 1c) are available. Two numerical experiments, EXP8 (wave-only simulation) and EXP9 (coupled wave-ice simulation), were performed. For EXP9, both ice-induced wave attenuation and blocking effect of ice on waves were considered, and the IC4M6 was used to estimate ice-induced wave attenuation because this method approximately represented an average of IC4M1–M7 (Fig. 6b–h).

Figure 7 a, c, and e show comparisons of the EXP8- and EXP9-modeled SWH with AWAC observations at stations 4a, 5a, and 6a in February 2011, respectively; meanwhile, the comparisons between the EXP9-modeled ice concentration and the NIC product for stations 4a, 5a, and 6a are displayed in Fig. 7 b, d, and f, respectively; on the basis of the changing trends in the SWH and ice concentration, three representative time slots, Period 1 (February 01–February 14, 2011), Period 2 (February 18–February 20, 2011), and Period 3 (February 23–March 02, 2011) were selected for further discussions, and these periods are marked with cyan, yellow, and gray shading in Fig. 7, respectively.

In Period 1, high ice concentration was revealed by both the NIC product (approximately 90%) and EXP9 simulation (approximately 100%) at all three AWAC stations (Fig. 7 b, d, and f). The AWAC wave observations showed that magnitudes of the SHW at stations 4a, 5a, and 6a were generally zero, which was accurately modeled by the coupled wave-ice experiment EXP9, while the wave-only case EXP8 produced completely incorrect simulation of the SWH (Fig. 7 a, c, and e). The detailed statistics (including RMSE and MAE) of SWH comparisons during Period 1 are listed in Table 3, again suggesting good performance of EXP9 in simulating the SWH under heavy-ice condition.

In Period 2, as indicated by Fig. 7 b, d, and f, remarkable decreases in ice concentration happened at all three AWAC stations. During this period, large SWH (even exceeds 2 m) were observed at stations 4a, 5a, and 6a, the large SWH possibly indicates that high winds strike Lake Erie, leading to strong mixing in the entire water column, bringing up the warm water from below, and finally melting the ice. Moreover, "ice retreat-wave growth" positive feedback may establish during this period: the melt of ice enlarges the area of open waters, directly facilitating the growth of waves, while the strengthened wave dissipation will induce ice breakage, accelerating the melting of ice, forming a positive feedback

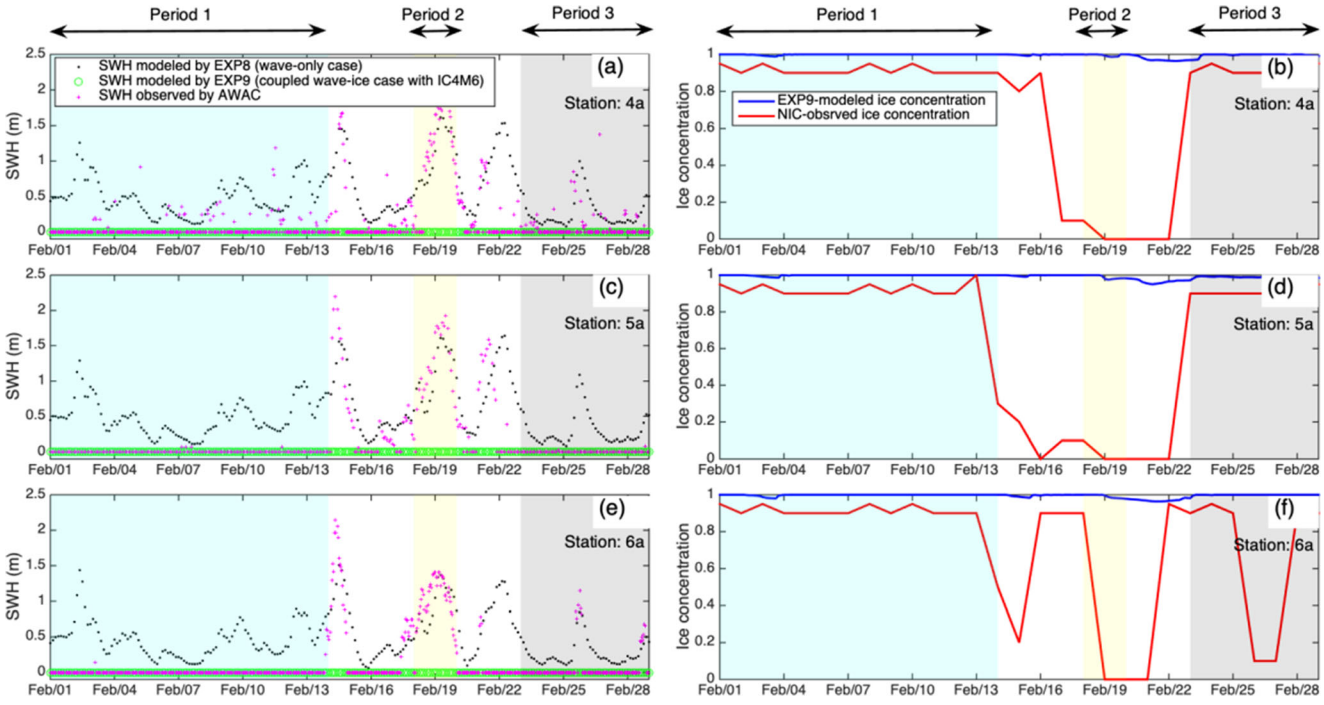

Fig. 7 Comparisons of the EXP8- and EXP9-modeled SWH with observations by AWAC at stations 4a (**a**), 5a (**c**), and 6a (**e**) in February 2011. The comparisons between the EXP9-modeled ice concentration and the NIC product at stations 4a (**b**), 5a (**d**), and 6a (**f**), respectively. Cyan, yellow, and gray shadings mark off Period 1 (February 01–February 14, 2011), Period 2 (February 18–February 20, 2011), and Period 3 (February 23–March 02, 2011), correspondingly

Table 3 Statistics of wave comparisons between EXP8 and EXP9 simulations with the AWAC observations during Period 1, 2, and 3 at stations 4a, 5a, and 6a

		Period 1		Period 2		Period 3	
		RMSE (m)	MAE (m)	RMSE (m)	MAE (m)	RMSE (m)	MAE (m)
Station 4a	EXP8	0.54	0.47	*0.47*	*0.43*	0.34	0.27
	EXP9	*0.05*	*0.01*	1.32	1.11	*0.15*	*0.04*
Station 5a	EXP8	0.55	0.48	*0.40*	*0.36*	0.37	0.30
	EXP9	*0.01*	*0.00*	1.25	1.14	*0.01*	*0.00*
Station 6a	EXP8	0.52	0.46	*0.35*	*0.28*	0.27	0.23
	EXP9	*0.06*	*0.01*	1.02	0.95	*0.20*	*0.05*

Better statistical results are highlighted with italics

(Zhang et al. 2020). Figure 7 a, c, and e prove that when ice concentration is below 10% or even zero, wave dynamics will be generally free of influence by ice, which explains why the SWH modeled by the wave-only case EXP8 agreed well with the observations. Note that EXP9 failed to reproduce the strong melting process during this period (Fig. 7 b, d, and f) and therefore, remarkably underestimated the SWH (Fig. 7 a, d, and e); this may be due to the low spatial resolution of the model, the errors in the NARR forcing, and the neglect of wave-induced ice breakage.

During Period 3, when high ice concentration (> 80%) covered all three AWAC stations, the results were much similar to that during Period 1, and the statistics summarized in Table 3 again suggest reasonable simulation of SWH by EXP9. Around February 14, 19, and 26, 2011, there were three significant decreases in ice concentration at station 6a, and each decrease lasted for about 3 days (Fig. 7f); as Fig. 7e reveals, the waves responded quite quickly to these ice-decreased events, suggesting a sensitive relationship between waves and ice.

5 Summary and conclusions

To better understand how waves and ice interact with each other in the Great Lakes, we developed a partly coupled wave-ice interaction model with the ability to resolve the ice-induced wave attenuation within the FVCOM framework. The WAVEWATCH III® IC4 was utilized to quantify the wave energy loss when propagating under ice. Meanwhile, the blocking effect of ice on wind energy input and wave energy decay via whitecapping and breaking were also implemented.

The model was then applied to the Great Lakes, and a set of numerical experiments were conducted to assess the reduction of wave height in the presence of ice. Numerical results demonstrated that the ice-induced wave attenuation and the ice concentration were positively correlated. In February 2014, there were almost no wind wave motions in Lakes Superior, Huron, and Erie because the heavy ice there could remarkably inhibit the growth and development of wind waves.

When validated by wave observations from bottom-moored AWAC in Lake Erie during an ice season, the model developed in this study satisfactorily reproduced the ice-attenuated waves. Analysis of the AWAC wave data and the satellite-retrieved ice concentration data indicated a quick response between waves and ice. Therefore, accurate ice modeling is necessary for resolving wave-ice interaction because there is a sensitive relationship between them.

In this study, the ice-induced wave attenuation in the Great Lakes was evaluated, and the significance of wave-ice interaction in the lake hydrodynamics was demonstrated. The partly coupled wave-ice interaction model provided a foundation for developing a fully coupled wave-ice-lake model for the Great Lakes. However, the feedbacks from waves to ice was not considered in the present investigation. Therefore, our model could not produce the “ice retreat-wave growth” process, which may be one of the main reasons for the modeling errors in Period 2 of Fig. 7. In the next stage, it would be interesting to implement effects of waves on ice into the model, e.g., wave-induced ice breakage. In addition, due to the high difficulty, technical requirements, and expenses of field observation in ice season, understanding of wave-ice interaction in the Great Lakes (also other cold regions) is limited by the scarcity of simultaneous wave and ice observations, and further field observations regarding wave-ice interaction under various ice and wave conditions are necessary in the future.

Acknowledgments We gratefully thank the two anonymous reviewers for providing constructive and insightful comments, which have contributed to the substantial improvements of the manuscript. Peng Bai acknowledges a grant from the National Research Council Research Associateship Programs. This research was partially funded by NSF Grant OCE 0927643 to Dmitry Beletsky. We would like to thank Songzhi Liu for his assistance in processing the NIC ice concentration data. This is GLERL Contribution No. 1946. Funding was awarded to the Cooperative Institute for Great Lakes Research (CIGLR) through the NOAA Cooperative Agreement with the University of Michigan (NA17OAR4320152). This CIGLR contribution number is 1160.

References

Allen RG, Pereira LS, Raes D, Smith M (1998) Crop evapotranspiration-guidelines for computing crop water requirements-FAO irrigation and drainage paper 56. Fao, Rome 300(9):D05109

Anderson E, Fujisaki-Manome A, Kessler J, Lang G, Chu P, Kelley J, Wang J (2018) Ice forecasting in the next-generation Great Lakes Operational Forecast System (GLOFS). J Mar Sci Eng 6(4):123

Ardhuin F, Roland A, Dumas F, Bennis A-C, Sentchev A, Forget P, Wolf J, Girard F, Osuna P, Benoit M (2012) Numerical Wave Modeling in Conditions with Strong Currents: Dissipation, Refraction, and Relative Wind. J Phys Oceanogr 42(12):2101–2120

Bai X, Wang J, Sellinger C, Clites A, Assel R (2012) Interannual variability of Great Lakes ice cover and its relationship to NAO and ENSO. J Geophys Res: Oceans 117(C3)

Bai X, Wang J, Schwab DJ, Yang Y, Luo L, Leshkevich GA, Liu S (2013) Modeling 1993–2008 climatology of seasonal general circulation and thermal structure in the Great Lakes using FVCOM. Ocean Model 65:40–63

Bai X, Wang J, Austin J, Schwab DJ, Assel R, Clites A, Wohlleben T (2015) A record-breaking low ice cover over the Great Lakes during winter 2011/2012: combined effects of a strong positive NAO and La Niña. Clim Dyn 44(5–6):1187–1213

Barber DG, Galley R, Asplin MG, De Abreu R, Warner KA, Pućko M, Julien S (2009) Perennial pack ice in the southern Beaufort Sea was not as it appeared in the summer of 2009. Geophys Res Lett 36(24)

Beletsky D, Saylor JH, Schwab DJ (1999) Mean circulation in the Great Lakes. J Great Lakes Res 25(1):78–93

Bennetts LG, Squire VA (2009) Wave scattering by multiple rows of circular ice floes. J Fluid Mech 639:213–238

Bennetts LG, Squire VA (2011) On the calculation of an attenuation coefficient for transects of ice-covered ocean. Proceedings of the Royal Society A: Mathematical, Physical and Engineering Sciences 468(2137):136–162

Booij NRRC, Ris RC, Holthuijsen LH (1999) A third-generation wave model for coastal regions: 1. Model description and validation. J Geophys Res Oceans 104(C4):7649–7666

Brissette FP, Tsanis IK, Wu J (1993) Wave directional spectra and wave-current interaction in Lake St. Clair. J Great Lakes Res 19(3):553–568

Brown RW, Taylor WW, Assel RA (1993) Factors affecting the recruitment of lake whitefish in two areas of northern Lake Michigan. J Great Lakes Res 19(2):418–428

Campbell AJ, Bechle AJ, Wu CH (2014) Observations of surface waves interacting with ice using stereo imaging. J Geophys Res Oceans 119(6):3266–3284

Chen C, Liu H, Beardsley RC (2003) An unstructured grid, finite-volume, three-dimensional, primitive equations ocean model: application to coastal ocean and estuaries. J Atmos Ocean Technol 20(1):159–186

Collins CO, Rogers WE (2017) A source term for wave attenuation by sea ice in WAVEWATCH III®: IC4. NRL report NRL/MR/7320–17-9726, 25 pp. [available from www7320. Nrlssc. Navy. Mil/pubs. Php]

De Santi F, De Carolis G, Olla P, Doble M, Cheng S, Shen HH, Thomson J (2018) On the ocean wave attenuation rate in grease-pancake ice, a comparison of viscous layer propagation models with field data. J Geophys Res: Oceans 123(8):5933–5948

Doble MJ, De Carolis G, Meylan MH, Bidlot JR, Wadhams P (2015) Relating wave attenuation to pancake ice thickness, using field measurements and model results. Geophys Res Lett 42(11):4473–4481

Dumont D, Kohout A, Bertino L (2011) A wave-based model for the marginal ice zone including a floe breaking parameterization. J Geophys Res: Oceans 116(C4)

Fujisaki-Manome A, Wang J (2016) Simulating hydrodynamics and ice cover in Lake Erie using an unstructured grid model. *Proceedings of 23th IAHR International Symposium on Ice* (2016)

Gao G, Chen C, Qi J, Beardsley RC (2011) An unstructured-grid, finite-volume sea ice model: development, validation, and application. Journal of Geophysical Research: Oceans 116(C8)

Hasselmann K, Barnett TP, Bouws E, Carlson H, Cartwright DE, Enke K, Meerburg A (1973) Measurements of wind-wave growth and swell decay during the Joint North Sea Wave Project (JONSWAP). Ergänzungsheft:8–12

Hawley N, Beletsky D, Wang J (2018) Ice thickness measurements in Lake Erie during the winter of 2010–2011. J Great Lakes Res 44(3):388–397

Horvat C, Tziperman E (2015) A prognostic model of the sea-ice floe size and thickness distribution. Cryosphere 9(6):2119–2134

Hubertz JM, Driver DB, Reinhard RD (1991) Wind waves on the Great Lakes: a 32 year hindcast. J Coast Res:945–967

Hunke EC, Lipscomb WH, Turner AK, Jeffery N, Elliott S (2010) CICE: the Los Alamos Sea ice model documentation and software User's manual version 4.1 LA-CC-06-012. T-3 Fluid Dynamics Group, Los Alamos National Laboratory, 675

Kohout AL, Meylan MH, Sakai S, Hanai K, Leman P, Brossard D (2007) Linear water wave propagation through multiple floating elastic plates of variable properties. J Fluids Struct 23(4):649–663

Kohout AL, Meylan MH (2008) An elastic plate model for wave attenuation and ice floe breaking in the marginal ice zone. J Geophys Res: Oceans 113(C9)

Kohout AL, Williams MJM, Dean SM, Meylan MH (2014) Storm-induced sea-ice breakup and the implications for ice extent. Nature 509(7502):604–607

Kohout AL, Williams MJM, Toyota T, Lieser J, Hutchings J (2016) In situ observations of wave-induced sea ice breakup. Deep-Sea Res II Top Stud Oceanogr 131:22–27

Komen GJ, Hasselmann K, Hasselmann K (1984) On the existence of a fully developed wind-sea spectrum. J Phys Oceanogr 14(8):1271–1285

Lou J, Schwab DJ, Beletsky D, Hawley N (2000) A model of sediment resuspension and transport dynamics in southern Lake Michigan. J Geophys Res: Oceans 105(C3):6591–6610

Madsen, O. S., Poon, Y. K., Graber, H. C. 1989. Spectral wave attenuation by bottom friction: theory. In *Coastal Engineering 1988* (pp. 492-504)

Mao M, Xia M (2017) Dynamics of wave–current–surge interactions in Lake Michigan: a model comparison. Ocean Model 110:1–20

Mao M, Van Der Westhuysen AJ, Xia M, Schwab DJ, Chawla A (2016) Modeling wind waves from deep to shallow waters in Lake Michigan using unstructured SWAN. J Geophys Res: Oceans 121(6):3836–3865

Mesinger F, DiMego G, Kalnay E, Mitchell K, Shafran PC, Ebisuzaki W, Ek MB (2006) North American regional reanalysis. Bull Am Meteorol Soc 87(3):343–360

Meylan MH, Bennetts LG, Kohout AL (2014) In situ measurements and analysis of ocean waves in the Antarctic marginal ice zone. Geophys Res Lett 41(14):5046–5051

Moeini MH, Etemad-Shahidi A (2007) Application of two numerical models for wave hindcasting in Lake Erie. Appl Ocean Res 29(3):137–145

Niimi AJ (1982) Economic and environmental issues of the proposed extension of the winter navigation season and improvements on the Great Lakes-St. Lawrence Seaway system. J Great Lakes Res 8(3):532–549

Niu Q, Xia M (2016) Wave climatology of Lake Erie based on an unstructured-grid wave model. Ocean Dyn 66(10):1271–1284

Niu Q, Xia M (2017) The role of wave-current interaction in Lake Erie's seasonal and episodic dynamics. J Geophys Res Oceans 122(9):7291–7311

Pleskachevsky A, Eppel DP, Kapitza H (2009) Interaction of waves, currents and tides, and wave-energy impact on the beach area of Sylt Island. Ocean Dyn 59(3):451–461

Qi J, Chen C, Beardsley RC, Perrie W, Cowles GW, Lai Z (2009) An unstructured-grid finite-volume surface wave model (FVCOM-SWAVE): Implementation, validations and applications. Ocean Model 28(1-3):153–166

Ris RC, Holthuijsen LH, Booij N (1999) A third-generation wave model for coastal regions: 2. Verification. J Geophys Res Oceans 104(C4): 7667–7681

Rogers WE, Thomson J, Shen HH, Doble MJ, Wadhams P, Cheng S (2016) Dissipation of wind waves by pancake and frazil ice in the autumn Beaufort Sea. J Geophys Res: Oceans 121(11):7991–8007

Schwab DJ, Beletsky D (2003) Relative effects of wind stress curl, topography, and stratification on large-scale circulation in Lake Michigan. J Geophys Res: Oceans 108(C2)

Sellinger CE, Stow CA, Lamon EC, Qian SS (2007) Recent water level declines in the Lake Michigan− Huron System. Environ Sci Technol 42(2):367–373

Squire VA (2007) Of ocean waves and sea-ice revisited. Cold Reg Sci Technol 49(2):110–133

The WAVEWATCH III® Development Group (WW3DG) (2016) User manual and system documentation of WAVEWATCH III® version 5.16. Tech. Note 329, NOAA/NWS/NCEP/MMAB, College Park, MD, USA, 326 pp. + Appendices

Vanderploeg HA, Bolsenga SJ, Fahnenstiel GL, Liebig JR, Gardner WS (1992) Plankton ecology in an ice-covered bay of Lake Michigan: utilization of a winter phytoplankton bloom by reproducing copepods. Hydrobiologia 243(1):175–183

Vaughan GL, Squire VA (2011) Wave induced fracture probabilities for arctic sea-ice. Cold Reg Sci Technol 67(1-2):31–36

Vavrus S, Notaro M, Zarrin A (2013) The role of ice cover in heavy lake-effect snowstorms over the Great Lakes Basin as simulated by RegCM4. Mon Weather Rev 141(1):148–165

Vincent CE (1979) The Interaction of Wind-Generated Sea Waves with Tidal Currents. J Phys Oceanogr 9(4):748–755

Wadhams P, Squire VA, Goodman DJ, Cowan AM, Moore SC (1988) The attenuation rates of ocean waves in the marginal ice zone. J Geophys Res: Oceans 93(C6):6799–6818

Wang J (1996) Global linear stability of the two-dimensional shallow-water equations: an application of the distributive theorem of roots for polynomials on the unit circle. Mon Weather Rev 124(6):1301–1310

Wang J, Ikeda M (1997a) Inertial stability and phase error of time integration schemes in ocean general circulation models. Mon Weather Rev 125(9):2316–2327

Wang J, Ikeda M (1997b) Diagnosing ocean unstable baroclinic waves and meanders using the quasigeostrophic equations and Q-vector method. J Phys Oceanogr 27(6):1158–1172

Wang R, Shen HH (2011) A continuum model for the linear wave propagation in ice-covered oceans: an approximate solution. Ocean Model 38(3–4):244–250

Wang J, Bai X, Hu H, Clites A, Colton M, Lofgren B (2012) Temporal and spatial variability of Great Lakes ice cover, 1973–2010. J Clim 25(4):1318–1329

Wang J, Kessler J, Bai X, Clites A, Lofgren B, Assuncao A, Leshkevich G (2018) Decadal variability of Great Lakes ice cover in response to AMO and PDO, 1963–2017. J Clim 31(18):7249–7268

Wang J, Manome A, Kessler J, Zhang S, Chu P, Peng S, Zhu X, Anderson E (2020) Inertial instability and phase error in third- and fourth-stage predictor-corrector time integration schemes in ocean circulation models: application to Great Lakes modeling. Ocean Dynamics (submitted)

Williams TD, Bennetts LG, Squire VA, Dumont D, Bertino L (2013) Wave–ice interactions in the marginal ice zone. Part 1: theoretical foundations. Ocean Model 71:81–91

Wright DM, Posselt DJ, Steiner AL (2013) Sensitivity of lake-effect snowfall to lake ice cover and temperature in the Great Lakes region. Mon Weather Rev 141(2):670–689

Xue P, Pal JS, Ye X, Lenters JD, Huang C, Chu PY (2017) Improving the simulation of large lakes in regional climate modeling: two-way lake–atmosphere coupling with a 3D hydrodynamic model of the Great Lakes. J Clim 30(5):1605–1627

Zhang Y, Chen C, Beardsley RC, Gao G, Qi J, Lin H (2016) Seasonal and interannual variability of the Arctic sea ice: a comparison between AO-FVCOM and observations. J Geophys Res: Oceans 121(11): 8320–8350

Zhang Y, Chen C, Beardsley RC, Perrie W, Gao G, Zhang Y, Lin H (2020) Applications of an unstructured grid surface wave model (FVCOM-SWAVE) to the Arctic Ocean: the interaction between ocean waves and sea ice. Ocean Model 145:101532